CRYSTAL GROWTH & DESIGN
2006
VOL. 6, NO. 1
327−334

# Nucleation Kinetics of Calcium Phosphates on Polyelectrolyte Multilayers Displaying Internal Secondary Structure

Vincent Ball,*[,†,‡] Marc Michel,[†] Fouzia Boulmedais,[‡] Joseph Hemmerle,[‡] Youssef Haikel,[‡] Pierre Schaaf,[†] and Jean Claude Voegel[‡]

*Institut Charles Sadron, Centre National de la recherche Scientifique, Unité Propre 22, 6 rue Boussingault, 67083 Strasbourg Cedex, France, and Institut National de la Santé et de la Recherche Médicale, Unité 595, Faculté de Chirurgie Dentaire, 11 rue Humann, 67085 Strasbourg Cedex, France*

*Received February 3, 2005; Revised Manuscript Received August 11, 2005*

**ABSTRACT:** The understanding of the role of biological macromolecules in the nucleation of calcium carbonates and calcium phosphates is of primary importance for the development of biomimetic surfaces able to mimic the proteins used by living organisms to produce such composite materials. In this study we show how polyelectrolyte multilayers made from poly-L-lysine (PLL) as the polycation and from a mixture of two polyanions, poly-L-glutamic acid (PGA) and poly-L-aspartic acid (Pasp), at different ratios are able to affect the duration of the lag time preceding crystal growth at constant supersaturation. These polyelectrolyte multilayers appear as interesting candidates for biomimetic surfaces, since they display a content of $\beta$-sheets that can be controlled by changing the PGA proportion in the polyanion mixture. The duration of the lag times preceding fast crystal growth is measured in situ with three complementary techniques, namely quartz crystal microbalance with dissipation (QCM-D), optical waveguide lightmode spectroscopy (OWLS), and infrared spectroscopy in the attenuated total reflection mode (ATR-FTIR). The three techniques lead to comparable results, and ATR-FTIR spectroscopy allows us to demonstrate that the growing inorganic particles are calcium phosphates. The obtained mineral is most probably octacalcium phosphate or poorly crystalline hydroxyapatite, whatever the PGA content of the multilayer film. However, the duration of the lag time as well as the morphology of the obtained particles cannot be simply correlated with the $\beta$ sheet content of the multilayer film.

## Introduction

For a long time, crystallizations of calcium phosphates and of calcium carbonates on the surfaces of thin films have constituted model systems for understanding the role of the surface chemistry in the nucleation and crystal growth processes.[1,2] Hence, surfaces covered with proteins extracted from mollusk shells,[3] Langmuir−Blodgett films of surfactant molecules bearing different kinds of hydrophilic moieties,[4−8] and self-assembled monolayers of surfactant molecules on noble metal surfaces[9,10] were used to study the morphology and the polymorphism of the obtained minerals. These studies were relatively cumbersome, due to the difficulty in producing such surface modifications. About 10 years ago, the layer by layer assembly of polyelectrolytes on charged solid surfaces allowed the modification of the surfaces of solid materials in a very easy and reproducible way.[11] The driving force for the buildup of such multilayers is the charge overcompensation afforded by the deposition of the last polyelectrolyte layer.[12] These polyelectrolyte multilayers may be used in electrooptical devices,[13,14] can be doped with semiconducting particles,[15] and can be used as model biomaterials able to release drugs[16] or active peptides such as α-melanocortin covalently bound to poly-L-lysine, which was used to build the multilayer film.[17] According to the nature of the last deposited layer, either chitosan or dextran sulfate, it was found that the procoagulant or anticoagulant activity of the multilayer could be controlled.[18] In the field of biomaterials, it is interesting to use charged surfaces such as osteoinductive materials, as has already been shown.[19] Indeed, polystyrene sulfonate/poly(allylamine) (denoted $(PSS/PAH)_n$) multilayers have already been used to induce the growth of calcium phosphates. It has been shown that multilayers ending with either PSS or PAH possess the same ability to induce nucleation and crystal growth.[20] More precisely, on a PSS-ending film, the critical supersaturation to observe nucleation was equal to 5.75 mM for both calcium and phosphate (in these experiments the calcium to phosphate ratio was fixed and equal to 1), whereas this critical supersaturation was equal to 6.12 mM on a PAH-ending film.

Very recently it has been demonstrated that a single PEI layer can be used to concentrate $Ni^{2+}$ cations near a surface[21] and to induce fractal growth of nickel clusters after the reduction of $Ni^{2+}$. This demonstrates the remarkable ability of polyelectrolyte multilayers to decorate solid surfaces with inorganic structures.

It is the aim of this paper to use polyelectrolyte multilayers built from mixtures of two polyanions (poly-L-glutamic acid (PGA) and poly-L-aspartic acid) and a single polycation (poly-L-lysine) to induce nucleation and crystal growth of calcium phosphates. The buildup of such multilayers has already been described[22] and it appeared that such multilayers constructed from homopolypeptides contain secondary structural elements such as α helixes and $\beta$ sheets. In particular, it was found from infrared spectra in the total attenuated reflectance mode (ATR) that the intensity of the infrared band attributed to the $\beta$ structures (at 1610 and 1680 $cm^{-1}$) was rather constant, as long as the percentage of PGA contained in the film was higher than about 40%. This observation seems of particular interest, since it is known that numerous proteins implied in the biomineralization of calcium carbonates are rich in $\beta$ sheets.[3] In addition, a number of proteins which are of major importance for the nucleation and growth of biominerals seem to be present on the surface of a $\beta$ chitin layer which is known to adopt mostly a $\beta$ sheet conformation.[23] The $\beta$ chitin layer is covered by a

* To whom correspondence should be addressed at the Institut Charles Sadron, Centre National de la recherche Scientifique. Email: ball@ics.u-strasbg.fr. Tel: 0033-3-88-41-40-12. Fax: 0033-3-88-41-40-99.
† Institut Charles Sadron, Centre National de la recherche Scientifique.
‡ Institut National de la Santé et de la Recherche Médicale. Tel: 0033-3-90-24-33-87.

10.1021/cg050044p CCC: $33.50 
Published on Web 09/20/2005

monolayer of acidic proteins onto which the nucleation and crystal growth of calcium carbonates takes place. The possibility of using such surfaces with tuned composition and conformation in order to control the nucleation and crystal growth of calcium phosphates was the motivation of this work. It is also worth noting that two of the polyelectrolytes used, PGA and PLL, having molecular weights different from those used in the present study, were investigated with respect to their ability to induce calcium phosphate crystal growth and phase transformation in the solution state.[24]

It is also interesting to note that when phosphoryn is adsorbing on the surface of HAP, the Pasp residues adopt a $\beta$ sheet conformation.[25] This shows that the $\beta$ sheet conformation is relevant not only for the growth of calcium carbonates but also for that of calcium phosphates. We will mainly focus on the measurement of the lag time duration preceding crystal growth: *hence, mainly on the kinetics of nucleation*. The duration of this lag phase was measured with three independent experimental techniques, namely quartz crystal microbalance with dissipation (QCM-D), optical waveguide lightmode spectroscopy (OWLS), and Fourier transform infrared spectroscopy in the attenuated total reflection mode (ATR-FTIR). This last experimental technique also allowed identification of the obtained minerals as calcium phosphates. The morphology of the resulting particles was furthermore investigated with scanning electron microscopy.

It came out from this investigation that the duration of the lag phase goes through a maximum when the polyelectrolyte multilayer contains about 40% PGA. Hence, the lag phase duration is not a single function of the $\beta$ structure content of the film. Nevertheless, it appears that films that are either rich in PGA or Pasp are good candidates for inducing rapid growth of calcium phosphates within a few hours. Moreover, the morphology of the obtained particles is also influenced by the PGA/Pasp content of the multilayers. The infrared spectra seem to be compatible with the presence of octacalcium phosphate (OCP) or poorly crystalline hydroxyapatite (HA), whatever the PGA or Pasp content of the film.

## Materials and Methods

The polyelectrolytes used to build the layer by layer polyelectrolyte films were all purchased from Sigma or Aldrich and used without further purification. The polycations, branched poly(ethyleneimine) (PEI, Aldrich Catalog No. 18,197-8, molecular weight 750 000 g $mol^{-1}$) and poly-L-lysine (viscosimetric molecular weight 57 900 g $mol^{-1}$) were dissolved at concentrations of 5 and 1 mg $mL^{-1}$, respectively, in 10 mM Tris (tris(hydroxymethyl)aminomethane, Gibco BRL) buffer adjusted to pH 7.4 with hydrochloric acid. This buffer also contained 150 mM sodium chloride (Prolabo). The polyanions, poly-L-glutamic acid (PGA, viscosimetric molecular weight 17 000 g $mol^{-1}$) and poly-L-aspartic acid (Pasp, viscosimetric molecular weight 33 400 g $mol^{-1}$) were dissolved at a total concentration of 1 mg $mL^{-1}$ in the same Tris-NaCl buffer.[22]

The calcium and phosphate solutions were prepared in the Tris-NaCl buffer at a total concentration of 12 mM. More precisely, the phosphate-containing solution was prepared by mixing $NaH_2PO_4 \cdot H_2O$ (Sigma, Catalog No. S-9638, lot 109H0194) and $Na_2HPO_4 \cdot 7H_2O$ (Sigma, Cat. S-9390, lot: 49H0418) at equimolar amounts. The resulting solution had a pH value of $6.85 \pm 0.05$. This pH reduction with respect to the Tris-NaCl buffer is due to the addition of phosphate ions to the solution. Just before the beginning of the nucleation and crystal growth experiment, the calcium-containing (in the form of anhydrous $CaCl_2$) and phosphate-containing solutions were put in an ultrasonic bath, filtered through 0.22 $\mu$m Millex (Millipore) membranes, and mixed volume to volume to yield a supersaturated calcium phosphate solution. This supersaturated solution did not yield any visible precipitate for at least 24 h. The absence of any calcium activity decrease was also checked in some experiments with a specific calcium electrode (ISE-K-40, Radiometer Analytical, the reference electrode being a saturated calomel electrode). In some experiments, however, visible precipitation occurred in the reservoir containing the supersaturated solution. These experiments were systematically discarded from data analysis.

**Quartz Crystal Microbalance with Dissipation (QCM-D).** The buildup of the polyelectrolyte multilayers and the measurement of the lag phase preceding the onset of crystal growth were followed by means of quartz crystal microbalance with dissipation, QCM-D. In this technique, one monitors the resonance frequencies of silica-coated quartz crystals as well as the dissipation factors at four frequencies (the fundamental close to 5 MHz, the third, fifth, and seventh harmonics close to 15, 25, and 35 MHz, respectively). These data allow us to follow the adsorption process in real time and to obtain some issues about the viscoelastic properties of the film, such as its shear viscosity and its shear modulus.[26−28] Provided the film is homogeneous, rigid, nonslipping and has a small thickness, the normalized frequency changes, $\Delta f/\nu$, where $\nu$ is an integer representing the harmonic number ($\nu = 1, 3, 5, 7$ for the first, third, fifth, and seventh harmonics, respectively), is proportional to the mass deposited on the crystal per unit area.[29]

The surface of the silica-covered quartz crystals (Q-Sense AB, Götenborg, Sweden) was cleaned with 2% (v/v) Hellmanex for 30 min in the sample cell of the quartz crystal microbalance (Q-Sense-AB, Götenborg, Sweden), rinsed with deionized water (Milli Q plus, Millipore, $\rho = 18.2$ MΩ cm), put in contact with a 0.1 M. hydrochloric acid solution, and finally intensively rinsed with the Tris-NaCl buffer. When a stable signal was reached ($\Delta f/\nu$ smaller than 1 Hz over a period of 1 min), 1 mL of the PEI solution was injected over the crystal surface and left at rest for 10 min. The buffer solution, 1 mL of the PGA, Pasp, or PGA/Pasp solution, the buffer solution, 1 mL of the PLL solution, and again the buffer solution were put into contact with the surface for 10 min each. For a given weight percentage $x$ of PGA in the polyanion mixture, one obtains the formation of a $\{PGA_z\text{-}Pasp_{1-z}\}$-PLL bilayer, *where z denotes the weight percentage of PGA effectively present in the polyelectrolyte multilayer*.

A 10 min contact between each solution and the surface was sufficient to reach a steady state in the adsorbed amounts.[22,30] After the deposition of the last PLL layer, the surface was rinsed again with the Tris-NaCl buffer and then with the flowing supersaturated calcium phosphate solution, which was injected through a Millex GV membrane at a flow rate of 1.45 $cm^3\ h^{-1}$. The alternating polycation and polyanion (or polyanion mixtures) led to PEI-$[(PGA_z\text{-}Pasp_{1-z})\text{-}PLL]_n$ architectures with $n$ equal to 6 or 6.5. Thus, films ending with PLL ($n = 6$) or with $PGA_z\text{-}Pasp_{1-z}$ ($n = 6.5$) were obtained. Some experiments were also performed in the case where $n = 3$ or $n = 8$.

**Optical Waveguide Experiments (OWLS).** The same multilayer films as those used in QCM-D were characterized in situ and in real time by means of optical waveguide lightmode spectroscopy (OWLS). This technique allows the determination of the optical thickness and the refractive index of an adsorbed layer on a $Si_{0.8}Ti_{0.2}O_2$ waveguiding substrate.[31] Briefly, a laser beam ($\lambda = 632.8$ nm) is directed on a diffraction grating imprinted in the waveguiding layer. For oxide films about 200 nm in thickness, only one transverse electric mode (TE) and one transverse magnetic mode (TM) are allowed to propagate along the waveguide.[32] This propagation is realized at discrete values of the incident angle of the laser beam by means of the diffraction grating. To each incoupling angle corresponds an effective refractive index $N_{TE}$ or $N_{TM}$. These values allow us to calculate the optical thickness $d_A$ and the refractive index $n_A$ of the film in the framework of a homogeneous and isotropic layer model, provided the thickness $d_F$ and refractive index $n_F$ of the waveguiding film have been previously calculated from the $N_{TE}$ and $N_{TM}$ values obtained when the waveguide is put in contact with buffer.[31,32] The OWLS technique is based on an evanescent wave, sensing the deposited film over a penetration depth of about 200−300 nm in our case (refractive index of the buffer $n_C = 1.334$, refractive index of the waveguiding film $n_F = 1.78$).

**Nucleation and Crystal Growth.** The supersaturated solution was flushed over the surface at a flow rate of either 1.45 mL $h^{-1}$ in the case of the OWLS and QCM-D experiments (syringue pusher, Razel, Bioblock Scientific, Illkirch, France) or 2.5 mL $h^{-1}$ in the case of the FTIR experiments. In all these experiments, the calcium and phosphate concentrations were equal to 6 mM each. The supersaturation ratios with respect to the possible calcium phosphate phases are given in Table 1. This study was performed at a supersaturation ratio clearly above that found in body fluids. Hence, the obtained results cannot be

**Table 1. Supersaturation Ratios with Respect to HAP, DCPD, and OCP for a Calcium Phosphate Solution at 6 mM ([$Ca^{2+}$]/[P] = 1) in the Presence of 10 mM Tris and 0.15 mM NaCl[a]**

| nature of the phase | DCPD | OCP | HAP |
|---|---|---|---|
| supersaturation with respect to this phase | 2.4 | 7.2 | 54 |

[a] See also Appendix I.

extrapolated to those that would be obtained in physiological situations. The ionic products were calculated using the activity coefficient $\gamma_i$ of ion *i* estimated with the extended Debye−Hückel formula proposed by Davies:[33]

$$\log \gamma_i = -0.509 z_i^2 \cdot I^{1/2}/(1 + I^{1/2}) \quad (1)$$

where *I* corresponds to the ionic strength of the solution and $z_i$ the valency of the considered ion. The formula used to calculate the ionic products of octacalcium phosphate (OCP), dicalcium phosphate dihydrate (DCPD), and hydroxyapatite (HAP) are given in Appendix I.

**Fourier Transform Infrared Spectroscopy in the ATR Mode.** The Fourier transform infrared spectroscopy (FTIR) experiments were performed on an Equinox 55 spectrometer (Bruker, Wissembourg, France) using a liquid nitrogen cooled detector. For the buildup of the multilayers, $D_2O$ was used as solvent instead of $H_2O$ because the amide I band of the polypeptides (between 1600 and 1700 $cm^{-1}$) is largely affected by the strong absorption of water around 1643 $cm^{-1}$ (O−H bending mode), whereas the corresponding vibration in $D_2O$ is around 1209 $cm^{-1}$.[34] All the spectra during the multilayer buildup were collected by accumulating 512 interferograms at 2 $cm^{-1}$ resolution. The spectra were decomposed as described in detail in previous publications[35] using the SPSERV software (SPSERV, version 3.20, Dr. Csaba Bagyinka, Institute of Biophysics, Biological Research Center of the Hungarian Academy of Sciences, P. O. Box 521, H6701 Szeged, Hungary).

The supersaturated solutions could not be prepared in $D_2O$ because of spontaneous precipitation. The reason for this spontaneous precipitation in $D_2O$ is not clear at the moment: it could be related to the different strengths of the hydrogen bonds in heavy water or to the presence of chemical impurities which would induce the appearance of nuclei in the supersaturated solution.. Hence, the supersaturated solutions had to be prepared in $H_2O$ solvent as for the OWLS and QCM-D experiments. This precluded the study of the influence of solutions simultaneously containing calcium and $H_2PO_4^-/HPO_4^{2-}$ ions on the conformation of the polyelectrolyte multilayer. Nevertheless, the influence of each individual ion on the average conformation of the multilayer film was investigated by flowing either calcium solutions or $H_2PO_4^-/HPO_4^{2-}$ solutions at 6 mM each on architectures previously defined with $n = 3, 6, 8$.

**Atomic Force Microscopy.** Architectures corresponding to $n = 3$, 6 were built by dipping 12 mm diameter glass slides alternatively in the polycation solution, in the Tris-NaCl buffer, in the polyanion solution (or in the $PGA_x$-$Pasp_{1-x}$ mixture), and again in the buffer solution. Each adsorption or rinsing step lasted over 10 min. The glass slides were cleaned just before the multilayer buildup, as for the optical waveguide experiments. At the end of the dipping procedure, the glass slides were stored in the Tris-NaCl buffer. Before imaging by AFM, they were quickly rinsed with distilled water, to remove the sodium chloride, and dried under a nitrogen stream. The slides where then imaged in the contact mode in air (Nanoscope III, Digital instruments) using silicon nitride cantilevers. The water rinse may have some effect on the morphology and structure of the obtained particles, since it induces some pH change. Nevertheless, this water rinse lasted for a few seconds only and its effect may be fairly limited, since its duration seems to be small in comparison with the characteristic times for structural changes in calcium phosphates.

**Scanning Electron Microscopy.** Some of the QCM-D crystals, covered with a multilayer and put in contact with a supersaturated solution, were rinsed with distilled water to remove the ions from the buffer, air-dried, and either sputter-coated (Hummer-Junior, Siemens, Germany) with a gold−palladium alloy or carbon-coated (JEOL JEE−4B Vacuum Evaporator, Japan). They were then imaged by SEM (JEOL JSM-35C, Japan) at accelerating voltages of the electrons of 25 or 15 kV.

**Optical Microscopy.** Several waveguides, modified with a polyelectrolyte multilayer and with inorganic particles grown after contact with a supersaturated solution, were imaged with a Nikkon TE 200 optical microscope connected to a video camera (SSC-M3, Sony, Japan). This was possible owing to the transparency of the waveguides.

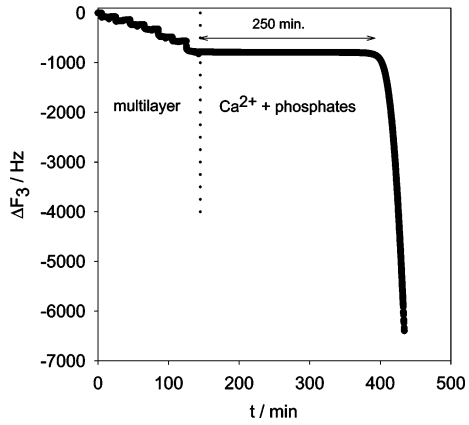


**Figure 1.** QCM-D experiment showing the frequency decrease close to 15 MHz during the PEI-$(PGA\text{-}PLL)_3$ multilayer buildup as well as during its exposure to a supersaturated calcium phosphate solution (6 mM in both calcium and phosphate ions in the Tris-NaCl buffer). The same kind of frequency change is observed close to 5, 25, and 35 MHz (data not shown).

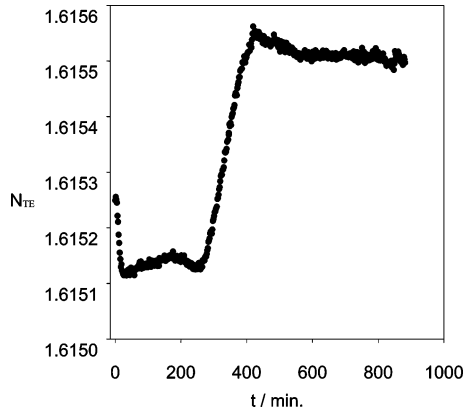


**Figure 2.** Evolution of the apparent refractive index corresponding to the transverse electric mode of the optical waveguide covered with a PEI-$(PGA\text{-}PLL)_3$ multilayer during its contact with a flowing (1.45 mL $h^{-1}$) supersaturated solution 6 mM in both calcium and phosphate ions. The flowing of the supersaturated solution began at $t = 0$. For clarity, the buildup of the PEI-$(PGA\text{-}PLL)_3$ multilayer has not been represented.

## Results and Discussion

After buildup of a PEI−$(PGA\text{-}PLL)_3$ film, the reproducibility of the induction times preceding fast crystal growth were first determined using three different techniques: QCM-D (Figure 1), OWLS (Figure 2) and ATR-FTIR spectroscopy (Figure 3). It comes as a first important observation that all three techniques detect a strong signal change after around 250 ± 20 min of contact between the polyelectrolyte multilayer and the supersaturated solution for this architecture (three bilayers). These changes correspond to a modification in both the resonance frequency (Figure 1) and the dissipation (data not shown) for the QCM-D experiments, a change in the phase velocity of both the TE (Figure 2) and TM (not shown) modes in the OWLS experiments, and the appearance of characteristic bands attributed to calcium phosphates[36,37] in the ATR-FTIR experiments (Figure 3). The ATR-FTIR experiments allow us to correlate the changes in the measured signals with the appearance of calcium phosphates. Hence, the period of time before these rapid

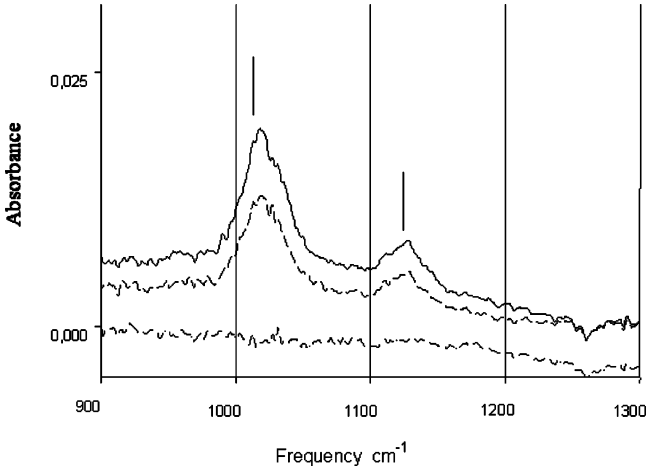


**Figure 3.** ATR-FTIR spectra showing the evolution of the phosphate bands between 900 and 1200 $cm^{-1}$ as a function of time after the injection of the supersaturated calcium phosphate solution (6 mM in calcium and phosphate ions in the Tris-NaCl buffer) over a PEI-(PGA-PLL)$_3$ multilayer. The bands centered at 1024 and 1126 $cm^{-1}$ have been indicated with vertical lines. The times at which the 512 scan spectra have been acquired were 213, 280, and 311 min (from bottom to top) after the beginning of the injection of the supersaturated solution.

changes corresponds to the lag time. The duration of this lag time will be called $\tau$ in the following. As will be seen later, the vibrational bands in the 900−1200 $cm^{-1}$ spectral domain furnish helpful information (but not definite conclusions) for the identification of the obtained calcium phosphates.

It has to be emphasized that a Tris-NaCl buffer solution containing only calcium or phosphate anions (at a concentration of 6 mM) did not induce any observable change in the amide I band of a PEI-(PGA-PLL)$_6$ polyelectrolyte multilayer (data not shown). This implies the absence of conformational changes in the polyelectrolyte multilayer as a consequence of the interactions between the calcium and phosphate ions with the polyelectrolytes. Moreover, when a PEI-(PGA-PLL)$_6$ or a PEI-(Pasp-PLL)$_6$ film is covered with an additional polyanion layer, rendering the multilayer negatively charged, the induction times were higher than 1500 min (the measurements were stopped after this period, and longer durations were not investigated). This clearly indicates, in this particular situation, that positively charged films are more able than negatively charged ones to induce nucleation and subsequent crystal growth. This is an interesting and rather unexpected observation, since it is well-known that negatively charged surfaces are more often encountered in nature as substrates for biomineralization.[1−3] However, polycations are also known to play an important role in some mineralization processes, such as in the silification of diatoms.[38] These results incited us to investigate the influence of the polyelectrolyte multilayer composition and hence its average conformation[22] on the duration of the lag phase preceding crystal growth. These experiments were realized on multilayers containing $n = 3$, 6, and 8 pairs of layers, all ending with PLL, and hence able to concentrate phosphate ions in their vicinity. The results are summarized in Table 2 and in Figure 4. Figure 4 represents both the evolution of $\tau$ with $z$ (the relative amount of PGA present in the multilayers, which can be calculated from the relative amount $x$ of PGA present in solution[22]) (Figure 4A) as well as the evolution of the relative intensity of the infrared bands attributed to $\beta$ sheets (Figure 4B). This relative intensity was estimated by means of a linear combination of the infrared spectra of pure (PGA-PLL) and of pure (Pasp-PLL) multilayers, as described previously.[22]

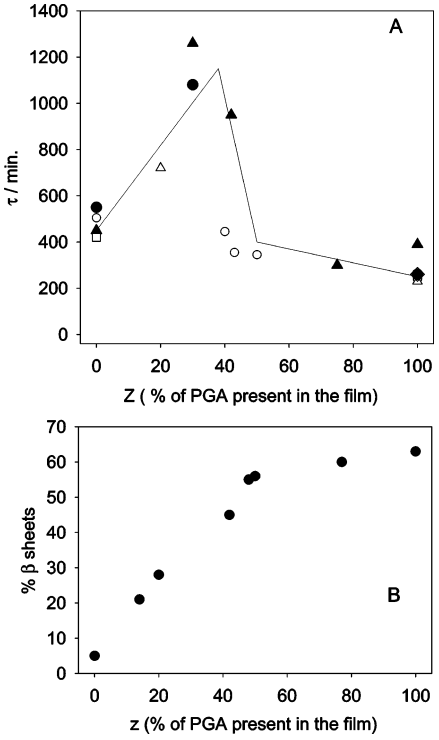


**Figure 4.** (A) Evolution of the induction time $\tau$ preceding crystal growth as a function of $z$: (○) QCM-D experiments for $n = 3$; (●) QCM-D experiments for multilayers made from 6 multilayers, (▲, △) ATR-FTIR experiments for $n = 3$, 6, respectively; (□) ATR-FTIR experiment performed on a PEI-(Pasp-PLL)$_8$ film; (◇) OWLS experiments performed on a PEI-(PGA-PLL)$_3$ film. The solid line is not a fit but is aimed to show the qualitative evolution of $\tau$ with $z$. (B) Evolution of the percentage of the $\beta$ sheet intensity in the amide I band as a function of $z$, the percentage of PGA present in the polyelectrolyte multilayer. The intensity of the $\beta$ sheet intensity is taken from figure 6 of ref 22.

**Table 2. Evolution of the Induction Times $\tau$ with Respect to $z$ for Variable Numbers of Deposited Multilayers, $n$**

| $z$ (PGA % in the multilayer) | $\tau$ (min) | no. of deposited bilayers | exptl technique |
|---|---|---|---|
| 100 | 290 | 3 | FTIR |
| 100 | 240 | 3 | QCM-D |
| 100 | 230 | 3 | FTIR |
| 100 | 260 | 3 | OWLS |
| 100 | 260 | 6 | QCM-D |
| 100 | 390 | 6 | FTIR |
| 75 | 300 | 6 | FTIR |
| 50 | 345 | 3 | QCM-D |
| 43 | 355 | 3 | QCM-D |
| 42 | 950 | 6 | FTIR |
| 40 | 445 | 3 | QCM-D |
| 30 | 1260 | 6 | FTIR |
| 30 | 1080 | 6 | QCM-D |
| 20 | 720 | 3 | FTIR |
| 0 | 505 | 3 | QCM-D |
| 0 | 450 | 3 | FTIR |
| 0 | 550 | 6 | QCM-D |
| 0 | 450 | 6 | FTIR |
| 0 | 420 | 8 | FTIR |

First of all, the measured lag times did not depend markedly on the thickness of the polyelectrolyte multilayer. This indicates that even with three pairs of layers, whose thickness is about 40 nm as estimated by OWLS,[39] the nucleation and crystal growth of calcium phosphates is not markedly influenced by the substrate, which indeed is different for QCM-D (quartz), for OWLS (a silica−titania mixture), and for ATR-FTIR (a ZnSe crystal). In this respect AFM images taken as described in

**Table 3. Comparison of the Peak Positions at the End of the Crystal Growth Period (Obtained from ATR-FTIR Experiments) with the Main Peak Positions Obtained from Reference Compounds[a]**

| sample and nature of the measurement | main peak positions ($cm^{-1}$) | compd |
|---|---|---|
| ref spectrum in the KBR mode | 1120, 1103, 1077, 1037, 1026, 962, 621, 601, 560, 537 | OCP |
| ref spectrum in the KBR mode | 1134, 1052, 994, 890, 562, 530 | DCPD |
| ref spectrum in the KBR mode | 1095, 1032, 962, 603, 563 | HAP |
| $z = 0\%$, $n = 3$[b] | 1120, 1015 | ? |
| $z = 0$, $n = 6$[b] | 1125, 1075, 1020 | OCP or poorly crystalline HAP |
| $z = 30\%$, $n = 6$,[b] KBR mode | 1120, 1105, 1077, 1037, 1024, 962, 944, 916, 626, 601, 560, 531 | OCP or poorly crystalline HAP |
| $z = 100\%$, $n = 3$[b] | 1125, 1110, 1035, 1020 | OCP or poorly crystalline HAP |
| $z = 80\%$, $n = 6$[b] | 1120, 1110, 1080, 1020 | OCP or poorly crystalline HAP |
| $z = 100\%$, $n = 3$[b] | 1125, 1110, 1035, 1020 | OCP or poorly crystalline HAP |
| $z = 100\%$, $n = 6$[b] | 1126, 1110, 1035, 1018 | OCP or poorly crystalline HAP |

[a] The last column indicates the compound corresponding to the best correspondence with the obtained spectra. [b] $n$ is the number of polyelectrolyte bilayers deposited on the surface.

Materials and Methods indicate that on films made from either three or six pairs of layers, with $x = 0$, 0.5, and 1, the root-mean-squared roughness never exceeds a few nanometers, with the absence of any observable holes going from the top of the film down to the silica substrate (data not shown). This also corroborates the probable absence of any kind of influence of the used substrate on the nucleation process. Moreover, a nucleation experiment was done by means of ATR-FTIR spectroscopy over a ZnSe crystal just coated by a PEI layer and put in contact with a supersaturated calcium phosphate solution (6 mM in calcium and phosphate in the presence of Tris-NaCl buffer). No increase in absorbance in the spectral region corresponding to the calcium phosphates was observed even after 24 h, a time duration significantly longer than all those observed on the thicker polyelectrolyte films. This indicates that a PEI layer is by itself not able to induce growth of calcium phosphates, at least in the investigated time range of 24 h.

From Figure 4 it appears that as long as the $\beta$ sheet intensity increases for $z$ increasing from 0 to about 40%, the values of $\tau$ also increase. The $\tau$ values then seem to reach a maximum value of about $1100 \pm 100$ min. Then, for higher values of $z$, when the $\beta$ sheet intensity reaches an almost constant value, $\tau$ decreases suddenly to values close to 300−400 min. Finally, for films containing only PGA as polyanion ($z = 100\%$), $\tau$ reaches a minimal value of $275 \pm 60$ min (mean value over six experiments). It is hence clear that nucleation proceeds faster on films containing only PGA as the polyanion than on films containing only Pasp ($\tau = 475 \pm 55$ min; mean value for five experiments). However, $\tau$ is not directly related to the intensity of the bands attributed to $\beta$ sheets in the infrared spectra. The occurrence of a maximum in the $\tau$ versus $z$ curve was unexpected. Indeed, we naively expected a regular decrease of $\tau$ with the increase of the $\beta$ sheet content, owing to a report by Addadi et al., who demonstrated that proteins rich in $\beta$ sheets are efficient promoters of calcium carbonates.[3] However, it appears that the maximum in the $\tau$ values occurs for PGA contents where the intensity of the $\beta$ sheet band reaches a plateau value (Figure 4B). One possible origin of this could be that, as long as the intensity of the $\beta$ sheet band increases, these $\beta$ sheets are not correctly oriented, which does not favor interactions with either the calcium or the phosphate ions. It is only when the $\beta$ sheet band intensity is close to its maximum value that certain amounts of the corresponding $\beta$ sheets are sufficiently well oriented to interact with the available ions. Another explanation could be that films containing about 40% PGA as a polyanion have a more pronounced inhibitory effect on the nucleation kinetics than films with another composition. The reason for this possible inhibition is not known, however.

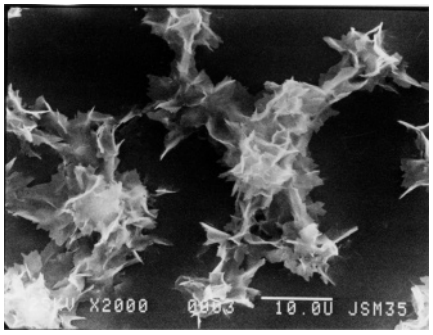


**Figure 5.** Scanning electron micrograph of a QCM-D crystal covered with a PEI-$(PGA\text{-}PLL)_3$ multilayer ($z = 100\%$), put in contact with a supersaturated solution (6 mM calcium and phosphate in the Tris-NaCl buffer), extensively rinsed with distilled water before metal deposition. The scale bar corresponds to 10 $\mu$m.

The infrared spectra clearly show that the obtained particles are calcium phosphates (Table 3). We attribute these bands to different calcium phosphates by comparing the obtained spectra with those of reference compounds. However, no visible bands appear in the ATR spectra in the spectral region between 700 and 900 $cm^{-1}$, which is also characteristic for the calcium phosphates.[36] This is due to the lack of transparency of the ZnSe crystal in this spectral range.

The SEM images obtained on the QCM-D quartz crystals, after water rinse, drying, and a thin metal layer deposition, show however that the morphology of the obtained particles changes importantly when $z$ varies from 100% (Figure 5) to 40% (Figure 6) to 0% (Figure 7). Moreover, some of the particles obtained for 40% of PGA in the film are broken after failure of part of their envelope (Figure 6B). The obtained morphology as well as the occurrence of broken fragments is reminiscent of that obtained by Bigi et al.[40] However, the particles we obtain are not hollow (Figure 6B), and Bigi et al. suggested that their hollow OCP capsules obtained in the presence of Pasp or polyacrylate polyanions in solution were obtained after dissolution of the central core to form a spherical shell constituted by radially oriented OCP plates. Hence, it seems that in the present case the crystal formation mechanism should be different from that proposed by Bigi et al.[40] The observation of complex three-dimensional architectures resembling those in Figure 6 were also recently observed in the case of copper hydroxide after ultrathin copper sheets were put in the presence of formamide.[41]

Thus, the present results clearly indicate a strong morphology change with the PGA content in the film. In the absence of Pasp (Figure 5), the morphology might well be that of octacalcium phosphate (OCP), whereas at lower PGA contents in the film (Figure 6), the morphology obtained is close to that

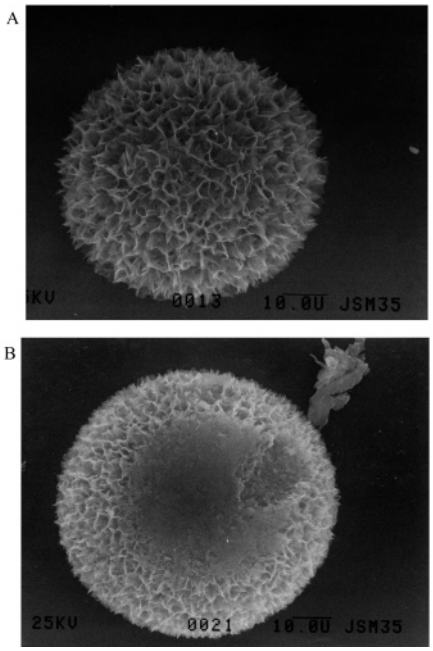


**Figure 6.** (A) Scanning electron micrograph of a QCM-D crystal covered with a PEI-({$PGA_{z=0.42}$-$Pasp_{1-z=0.58}$}-PLL)$_3$ multilayer, put in contact with a supersaturated solution (6 mM calcium and phosphate in the Tris-NaCl buffer), extensively rinsed with distilled water before metal deposition. The scale bar corresponds to 10 $\mu$m. (B) The same as in panel A, showing a partially broken sphere as well as a broken part coming from a sphere (upper right part).

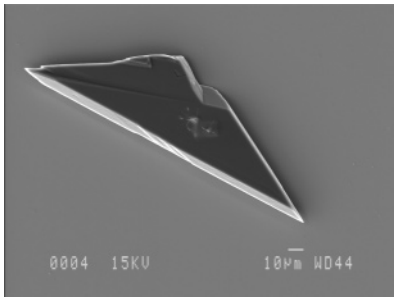


**Figure 7.** Scanning electron micrograph of a QCM-D crystal covered with a PEI-(Pasp-PLL)$_3$ multilayer ($z$ = 0%), put in contact with a supersaturated solution (6 mM calcium and phosphate in the Tris-NaCl buffer), extensively rinsed with distilled water before metal deposition. The scale bar corresponds to 10 $\mu$m.

observed by the group of Bigi.[40] The dendritic spherical particles observed in Figure 6 might possibly appear during the drying and exposure to high-vacuum conditions used for imaging in scanning electron microscopy. However, light microscopy observations confirm that the observed spherical particles constituted by radially oriented platelet particles are not due to artifacts induced before or during electron microscopy imaging (Figure 8). One observes also (Figure 7) that in the absence of PGA ($z$ = 0) very large platelet-shaped particles are formed.

For all the investigated architectures, it was not possible to collect enough material to perform X-ray diffraction experiments on the collected particles. Micro-diffraction experiments will be performed and presented in a forthcoming study. Hence, to correlate the morphology changes of the particles observed in Figures 5−7 for different PGA contents inside the film with their chemical and crystallographic characterizations, we used the data obtained from the ATR-FTIR spectra at the end of the growth phase. The attribution of the obtained calcium phosphate phases is hence only of a qualitative nature. The main infrared peaks are gathered in Table 3. For all the analyzed spectra, the main identified compound seems to be OCP, but one cannot totally exclude that these spectra could correspond to poorly crystalline HAP. As already mentioned previously, we were not able to collect the infrared spectra in the frequency domain between 500 and 700 cm$^{-1}$. Hence, on one of the samples used for the ATR-FTIR experiments, the ZnSe crystals were extensively and rapidly washed with distilled water and dried under a stream of nitrogen and the polyelectrolyte multilayer was crushed away and dried. The collected powder was again insufficient to perform X-ray diffraction but was sufficient to measure an infrared spectrum in the transmission KBr mode (Table 3). In this case, and in contrast to the measurements performed on the ZnSe crystal, a full spectrum could be obtained between 500 and 1200 cm$^{-1}$. For z = 30%, where $\tau$ is close to its maximum, the peaks obtained from the KBr spectra are again consistent with the occurrence of OCP (Table 3).

It has to be noted that these ATR-FTIR and KBr spectra were obtained after extensive exposure to water, which often promotes the phase transformation of OCP into HAP.[42] This is obviously not the case here. The calcium phosphates produced in this study were grown in the presence of polyelectrolytes, PLL, PGA, and Pasp, or a mixture of both polyanions. It has been shown that polyanions such as poly(acrylic acid) are able to inhibit the phase transformation of OCP into HAP.[42]

It appears that the obtained calcium phosphates are made from polycrystalline (Figures 5 and 6) particles. These seem to be made of octacalcium or poorly crystalline HAP (Table 3) for PGA contents in the multilayer between about 40% and about 100%. The morphology of the particles, namely aggregated flat platelets, is in agreement with that expected for OCP. Moreover, even in the total absence of PGA the observed large crystals were made of OCP.

It was partly unexpected that the absence of phase changes when $z$ changes from 0 to 100% was accompanied by a significant change in particle morphology, as shown in Figures 6−8. However, it is also well-known that the OCP formation is favored at the high supersaturations used in this study.

## Conclusion

In this study, we have shown that polyelectrolyte multilayers ending with PLL and made from either three, six, or eight bilayers in which the PGA content varies between 0 and 100% are able to initiate calcium phosphate nucleation and crystal growth. The induction times preceding crystal growth as measured by QCM-D, OWLS, and ATR-FTIR spectroscopy are very reproducible and display a maximum for films containing about 40% in PGA. Clearly the induction times are not simply related to the $\beta$ sheet contents found in the polyelectrolyte multilayers. Nevertheless, these induction times can be finely and reproducibly controlled by varying the composition of the polyelectrolyte multilayer. It seems, from the comparison of the induction time evolution with that of the $\beta$ sheet content, that the maximum value of $\tau$ is obtained for a film composition at which its $\beta$ sheet content reaches a plateau. The $\tau$ values then suddenly decrease with an increase in $z$, whereas the $\beta$ sheet content of the film only weakly increases. This observation warrants a complete study. However, it might well be that other effects contribute to the variation of $\tau$ with $z$. Effects such as complicated variation of the surface potential of the polyelectrolyte multilayer with $z$ or a phase segregation between regions rich in Pasp and regions rich in PGA could also play a major role in the nucleation. Indeed, a multilayer made purely of Pasp

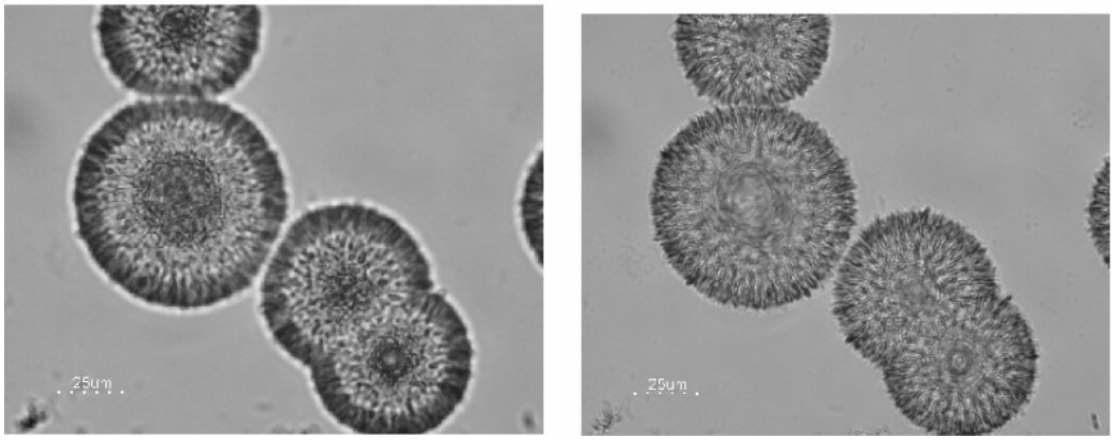


**Figure 8.** Optical micrograph of the particles grown on a PEI-({$PGA_{z=0.42}-Pasp_{1-z=0.58}$}-PLL)$_3$ multilayer on the surface of an optical waveguide. The two images were obtained by slightly changing the focus plane.

induces crystal growth after an induction time of 475 ± 55 min, whereas a multilayer made of PGA alone induces crystal growth after a significantly shorter induction time of 275 ± 60 min. We were not able to characterize the obtained minerals by means of electron diffraction or X-ray diffraction methods, but in situ ATR-FTIR measurements, as well as measurements made with the KBR method, showed that the infrared spectra are very close to those of octacalcium phosphate (OCP) or poorly crystalline HAP. Moreover, the morphologies obtained by SEM in the composition range between $z = 40$ and $z = 100\%$ are also in agreement with the OCP formation. However, at $z = 0\%$ (films containing only Pasp), a significant change in morphology is observed. At the present stage, we do not have a clear explanation for this observation. The possible formation of OCP rather than the more stable HAP, even after extensive exposure to water, indicates that the presence of the polyelectrolyte multilayers or of the polyelectrolytes themselves may inhibit the phase transformation of the obtained particles.

## Appendix

The ionic compositions of HAP, DCPD, and OCP correspond to $Ca_5(PO_4)_3OH$, $CaHPO_4{\cdot}2H_2O$, and $Ca_4H(PO_4)_3{\cdot}2.5H_2O$, respectively. Their ionic products can then be defined as

$$IP_{HAP} = \{a(Ca^{2+})\}^5\{a(PO_4^{3-})\}^3\{a(OH^-)\} \quad (2)$$

$$IP_{DCPD} = \{a(Ca^{2+})\}\{a(HPO_4^{2-})\} \quad (3)$$

$$IP_{OCP} = \{a(Ca^{2+})\}^4\{a(PO_4^{3-})\}^3\{a(H^+)\} \quad (4)$$

In eqs 2−4, $\{a(X)\}$ corresponds to the activity of the ionic species X. According to the molecular formulas of the different calcium phosphate compounds, the supersaturation ratios with respect to these compounds are defined by

$$S_{HAP} = (IP_{HAP}/K_{S,HAP})^{1/9} \quad (5)$$

$$S_{DCPD} = (IP_{DCPD}/K_{S,DCPD})^{1/2} \quad (6)$$

$$S_{OCP} = (IP_{OCP}/K_{S,OCP})^{1/8} \quad (7)$$

where the $K_S$ values are the solubility products of the corresponding samples.

Hence, to calculate the supersaturation ratios, the activities of the different ions have to be calculated. This requires the estimation both of the activity coefficients and of the fraction of the phosphate anions which exist in the corresponding form since the different phosphate species are in equilibrium.

The calculation of the activity coefficients is done by the use of eq 1.

The mass conservation of the phosphate species can be written as

$$[P] = [H_3PO_4] + [H_2PO_4^-] + [HPO_4^{2-}] + [PO_4^{3-}] \quad (8)$$

where [P] is the total concentration of phosphate anions. The concentrations of all these species are related by chemical equilibria:

$$H_3PO_4 \leftrightarrow H^+ + H_2PO_4^- \quad \text{equilibrium constant } K_1 \quad (9)$$

$$H_2PO_4^- \leftrightarrow H^+ + [HPO_4^{2-}] \quad \text{equilibrium constant } K_2 \quad (10)$$

$$[HPO_4^{2-}] \leftrightarrow H^+ + [PO_4^{3-}] \quad \text{equilibrium constant } K_3 \quad (11)$$

The values of these equilibrium constants at 298 K are:

$$K_1 = 6.53 \times 10^{-3}\ \text{mol L}^{-1}\ ^{43}$$

$$K_2 = 6.57 \times 10^{-8}\ \text{mol L}^{-1}\ ^{44}$$

$$K_3 = 4.73 \times 10^{-13}\ \text{mol L}^{-1}\ ^{45}$$

The fraction of the phosphate species which exists at the actual pH value of the solution in the form of $PO_4^{3-}$ is given by

$$F(PO_4^{3-}) = [PO_4^{3-}]/[P] \quad (12)$$

Using the definition of the equilibrium constants as they appear from eqs 9−11, one obtains

$$F(PO_4^{3-}) = K_1K_2K_3/(Q\gamma_{PO_4^{3-}}) \quad (13)$$

with

$$Q = \{a(H^+)\}^3 + K_1\{a(H^+)\}^2/\gamma_{H_2PO_4^-} + K_1K_2\{a(H^+)\}/\gamma_{HPO_4^{2-}} + K_1K_2K_3/\gamma_{PO_4^{3-}} \quad (14)$$

being the fraction of phosphate species in the form of $PO_4^{3-}$

In eq 14, $\gamma_X$ values are the activity coefficients of species X.

The corresponding fractions for the $HPO_4^{2-}$ and $H_2PO_4^-$ species can also be defined. Using the ionic product of water, $K_W = 1.01 \times 10^{-14}$ at 298 K, the ionic products (eqs 2−4) can then be calculated from all the other equations. Then, using the values of the solubility products, namely $K_{S,HAP} = 1.18 \times 10^{-60}$,[46] $K_{S,DCPD} = 2.4 \times 10^{-7}$,[46] and $K_{S,OCP} = 5 \times 10^{-40}$,[46] the supersaturation ratios defined in eqs 5−7 can be calculated.

## References


(1) Mann, S. *Nature* **1988**, *332*, 119.
(2) Heywood, B. R.; Mann, S. *Adv. Mater.* **1994**, *6*, 9.
(3) (a) Addadi, L.; Moradian, J.; Shay, E.; Maroudas, N. G.; Weiner, S. *Proc. Natl. Acad. Sci. U.S.A.* **1987**, *84*, 2732. (b) Weiner, S.; Addadi, L. *J. Mater. Chem.* **1997**, *7*, 689.
(4) Mann, S.; Heywood, B. R.; Rajam, S.; Birchall, J. D. *Nature* **1988**, *334*, 692.
(5) Mann, S.; Didymus, J. M.; Sanderson, N. P.; Heywood, B. R.; Samper, E. J. A. *J. Chem. Soc., Faraday Trans.* **1990**, *86*, 1873.
(6) Rajam, S.; Heywood, B. R.; Mann, S. *J. Chem. Soc., Faraday Trans.* **1991**, *87*, 727.
(7) Buijnsters, P. J. J. A.; Donners, J. J. J. M.; Hill, S. J.; Heywood, B. R.; Nolte, R. J. M.; Zwanenburg, B.; Sommerdijk, N. A. J. M. *Langmuir* **2001**, *17*, 3623.
(8) Zhang, L. J.; Liu, H. G.; Feng, X. S.; Zhang, R. J.; Zhang, L.; Mu, Y. D.; Hao, J. C.; Qian, D. J.; Lou, Y. F. *Langmuir* **2004**, *20*, 2243.
(9) Küther, J.; Seshadri, R.; Knoll, W.; Tremel, W. *J. Mater. Chem.* **1998**, *8*, 641.
(10) (a) Aizenberg, J.; Black, A. J.; Whitesides, G. M. *Nature* **1999**, *398*, 495. (b) Aizenberg, J. *Dalton Trans.* **2000**, 3963.
(11) Decher, G. *Science* **1997**, *277*, 1232.
(12) Ladam, G.; Schaad, P.; Voegel, J. C.; Schaaf, P.; Decher, G.; Cuisinier, F. J. G. *Langmuir* **2000**, *16*, 1249.
(13) Fou, A. C.; Onitsuka, O.; Ferreira, M.; Rubner, M. F.; Hsieh, B. R. *J. Appl. Phys.* **1996**, *79*, 7501.
(14) Eckle, M.; Decher, G. *Nano Lett.* **2001**, *1*, 45.
(15) Kotov, N. A.; Dekany, I.; Fendler, J. H. *J. Phys. Chem.* **1995**, *99*, 13065.
(16) Benkirane-Jessel, N.; Schwinte, P.; Falvey, P.; Darcy, R.; Haïkel, Y.; Schaaf, P.; Voegel, J. C.; Ogier, J. *Adv. Funct. Mater.* **2004**, *14*, 174.
(17) Chluba, J.; Voegel, J. C.; Decher, G.; Erbacher, P.; Schaaf, P.; Ogier, J. *Biomacromolecules* **2001**, *2*, 800.
(18) Serizawa, T.; Yamaguchi, M.; Matsuyama, T.; Akashi, M. *Biomacromolecules* **2000**, *1*, 306.
(19) Hatgerink, J. D.; Beniash, E.; Stupp, S. I. *Science* **2001**, *294*, 1684.
(20) Ngankam, P. A.; Lavalle, P.; Voegel, J. C.; Szyk, L.; Decher, G.; Schaaf, P.; Cuisinier, F. J. G. *J. Am. Chem. Soc.* **2000**, *122*, 8998.
(21) Lee, I.; Ahn, J. S.; Hendricks, T. R.; Rubner, M. F.; Hammond, P. T. *Langmuir* **2004**, *20*, 2478.
(22) Debreczeny, M.; Ball, V.; Boulmedais, F.; Szalontai, B.; Voegel, J. C.; Schaaf, P. *J. Phys. Chem. B* **2003**, *107*, 12734.
(23) Kato, T. *Adv. Mater.* **2000**, *12*, 1543.
(24) Bar-Yosef Ofir, P.; Govrin-Lippman, R.; Garti, N.; Füredi-Milhofer, H. *Cryst. Growth Des.* **2004**, *4*, 177.
(25) Fujisawa, R.; Kuboki, Y. *Eur. J. Oral Sci.* **1998**, *106*, 249.
(26) Rodahl, M.; Kasemo, B. *Sens. Actuators, A* **1996**, *54*, 448.
(27) Voinova, M. V.; Rodahl, M.; Jonson, M.; Kasemo, B. *Phys. Scr.* **1999**, *59*, 391.
(28) Höök, F.; Kasemo, B.; Nylander, T.; Fant, C.; Sott, K.; Elwing, H. *Anal. Chem.* **2001**, *73*, 5796.
(29) Sauerbrey, G. *Z. Phys.* **1959**, *155*, 206.
(30) Boulmedais, F.; Ball, V.; Schwinte, P.; Frisch, B.; Schaaf, P.; Voegel, J. C. *Langmuir* **2003**, *19*, 440.
(31) Tiefenthaler, K.; Lukosz, W. *J. Opt. Soc. Am. B: Opt. Phys.* **1989**, *6*, 209.
(32) Picart, C.; Ladam, G.; Senger, B.; Voegel, J. C.; Schaaf, P.; Cuisinier, F. J. G.; Gergely, C. *J. Chem. Phys.* **2001**, *115*, 1086.
(33) Davies, C. W. *Ion Association*, Butterworths: London, 1962.
(34) Venyaminov, S.; Kalnin, N. N. *Biopolymers* **1990**, *30*, 1259.
(35) Schwinte, P.; Ball, V.; Szalontai, B.; Haikel, Y.; Voegel, J.-C.; Schaaf, P. *Biomacromolecules* **2002**, *3*, 1135.
(36) Koutsopoulos, S. *J. Biomed. Mater. Res.* **2002**, *62*, 600.
(37) Elliott, J. C. *Studies Inorg. Chem.* **1994**, *18*, page 171.
(38) Kröger, N.; Deutzmann, R.; Sumper, M. *Science* **1999**, *286*, 1129−1132.
(39) Lavalle, P.; Gergely, C.; Cuisinier, F. J. G.; Decher, G.; Schaaf, P.; Voegel, J. C.; Picart, C. *Macromolecules* **2002**, *35*, 4458.
(40) Bigi, A.; Boanini, E.; Walsh, D.; Mann, S. *Angew. Chem.* **2002**, *114*, 2267.
(41) Zhang, Z.; Shao, X.; Yu, H.; Wang, Y.; Han, M. *Chem. Mater.* **2005**, *17*, 332.
(42) Bigi, A.; Boanini, E.; Falini, G.; Panzavolta, S.; Roveri, N. *J. Inorg. Biochem.* **2000**, *78*, 227.
(43) Nims, L. F. *J. Am. Chem. Soc.* **1934**, *56*, 1110.
(44) Bates, R. G.; Acree, S. F. *J. Res. Natl. Bur. Stand. U.S.A.* **1943**, *30*, 129.
(45) *Handbook of Chemistry and Physics*, 67th ed.; CRC Press: Boca Raton, FL, 1986; p D-163.
(46) Gramain, P.; Voegel, J. C.; Gumpper, M.; Thomann, J. M. *J. Colloid Interface Sci.* **1987**, 118.


CG050044P